Enhanced Capacity and Easily Separable Adsorbent of Dithizone-immobilized Magnetite Zeolite for Pb(II) Adsorption

Carissa Ayu Susiana, Bambang Rusdiarso, and Mudasir Mudasir*

Department of Chemistry, Faculty of Mathematics and Natural Sciences, Universitas Gadjah Mada, Sekip Utara, Yogyakarta 55281, Indonesia

*** Corresponding author:**

email: mudasir@ugm.ac.id

Received: November 21, 2023
Accepted: April 26, 2024

DOI: 10.22146/ijc.90914

Abstract: *In this study, magnetic natural zeolite (ZTM) was prepared using the coprecipitation method and dithizone was then immobilized on its surface in less toxic medium of alkaline to yield dithizone-immobilized magnetic zeolite (ZTM-Dtz). The synthesized ZTM-Dtz was characterized by FTIR and XRD, indicating that dithizone was successfully immobilized on the surface of ZTM. Vibrating sample magnetometer measurements showed superparamagnetic properties of either ZTM or ZTM-Dtz with magnetization values of 7.35 and 11.49 emu g^{-1}, respectively. The adsorption kinetics of Pb(II) on both adsorbents followed a pseudo-second-order and their adsorption isotherms were properly described by the Langmuir model. The adsorption capacity of ZTM and ZTM-Dtz were 6.94 and 38.46 mg g^{-1}, respectively, suggesting that dithizone immobilization enhanced the adsorbent capacity more than 5 times. The interaction mechanism between Pb(II) metal ion and ZTM was dominated by ion exchange, whereas that of ZTM-Dtz was mostly hydrogen bonds and complexation. The synthesized material is promising to be developed for the adsorption of heavy metal ions such as Pb(II) because it provides a high adsorption capacity and the adsorbents can be easily separated magnetically after application.*

Keywords: *magnetic zeolite; dithizone; Pb(II) ions; adsorption; desorption*

■ INTRODUCTION

Human activities such as mining and industries produce many wastes, one of which is heavy metal ions. These metal ions are dangerous persistent pollutants with toxic properties that are not easily decomposed and can bioaccumulate in the human body [1]. Lead (Pb) metal and its compounds are widely used in pipe manufacturing, battery recycling, exhaust manufacturing, and the paint industry [2]. Pb is a toxic heavy metal ion that can interfere with our health by disturbing the metabolism of kidneys, nerve, anemia, gastrointestinal, and blood vessel damage [3].

Studies show that several methods can be used to remove Pb(II) in the environment, including chemical precipitation, electrocoagulation, adsorption, membrane filtration, and ion exchange [4-5]. Among these methods, adsorption seems to be the most promising method for removing heavy metal ions due to its advantages including low cost, high efficiency, and easy application. So far, zeolite has been widely selected as an adsorbent because it has cation exchange properties with a porous framework structure, cavities, and a large surface area. Modification of zeolites is still needed to improve their selectivity and capacity towards certain metal ions. Moreover, the serious problem that is always encountered when using the adsorption method to remove pollutants is the separation of the adsorbent from the system after application. Therefore, an easy method of adsorbent separation should be introduced, for example by magnetizing the adsorbent so that it can be easily separated by an external magnet after application [6].

In the present study, we have modified the surface of the zeolites with dithizone to enhance their selectivity towards Pb(II), followed by magnetization of the zeolites to make separation easier after application. The modification procedure includes acid activation [7],

magnetization of activated zeolite [8], and dithizone immobilization of magnetic zeolite [9]. Dithizone has been chosen as an organic ligand to be used for immobilization because it can easily react with some heavy metal ions to form metal-chelate complexes due to the presence of electron-donating groups such as –NH and –SH in its structure [10-11].

Recently, research on dithizone immobilization on the surface of the host materials has been widely developed. For example, dithizone has been immobilized on the surface of bentonite and showed a higher sorption selectivity to Hg(II) and Zn(II) even in the presence of other metal ions with similar charges and sizes, such as Mg(II) and Ca(II) ions. So far, the immobilization of dithizone to the host material is always done in organic solvents such as toluene, carbon tetrachloride, and chloroform because dithizone ligands dissolve well in these solvents. However, their toxic and flammable properties are not desirable with respect to the principles of green chemistry [12-20]. In addition, non-polar organic solvents cannot wet the surface of the adsorbent whose active site contains polar silica-alumina, so the interaction between dithizone and the adsorbent site does not work perfectly.

As an alternative method, Huda et al. [9] reported the immobilization of dithizone on coal bottom ash in water/base medium. The adsorption capacity of the modified coal bottom ash towards Pb(II) ions increased almost 3 times higher than that of the unmodified one. The formation of the anionic dithizone species when it is dissolved in a water/alkaline medium makes it easier for the immobilization process on the polar surface of the supporting material due to the stabilization of cations from the solvent medium.

Therefore, in this research, we have used an eco-friendly dithizone immobilization technique on the surface of magnetized zeolite with magnetite (Fe_3O_4) in a water/alkaline medium with the aim that the resulting adsorbent is more sensitive and selective to the Pb(II) ions and after adsorption, it can be easily separated from the system by an external magnet. Some parameters that affect the Pb(II) adsorption, including solution pH, adsorbent mass, contact time and initial concentration of adsorbate, are systematically examined. From the obtained data, kinetics and isotherm adsorption models are also evaluated. Moreover, sequential desorption studies have also been conducted to understand better the type of interaction between the active sites of the adsorbent and Pb(II) ion. From this study, the adsorption properties of the synthesized adsorbent have been well understood. Therefore it has the potential to be further developed as a selective adsorbent of Pb(II) ion with high adsorption capacity.

■ EXPERIMENTAL SECTION

Materials

The materials used in the study included natural zeolites from Jogonalan, Klaten, Central Java. Chemicals of HCl (37%), HF, HNO_3, $FeSO_4{\cdot}7H_2O$, $FeCl_3{\cdot}6H_2O$, NH_3 (25%), dithizone, NaOH, $Pb(NO_3)_2$, KNO_3, $HONH_2HCl$, CH_3COOH (99%), and Na_2EDTA with pro-analytical quality (p.a.) were purchased from Merck, Germany. Distilled water and deionized water were obtained from CV Progo Mulyo and used for the experiment without further treatment.

Instrumentation

In this study, the characterization of materials was carried out using Fourier-transform infrared spectrophotometer (FTIR, IR Prestige-21, Shimadzu), the X-ray diffractometer (XRD, Bruker D8 Advance Eco) with CuKα radiation at $\lambda = 0.154$ nm and the vibrating sample magnetometer (VSM 250) instrument operated at room temperature using an external magnetic field range of H = 0.1–21 kOe. Meanwhile, analysis of Pb(II) in aqueous solution before and after adsorption was done using an atomic absorption spectrophotometer (AAS, Perkin Elmer 3110).

Procedure

Synthesis of magnetic zeolite

Natural zeolite was first acid-activated by refluxing it with HCl 6 M at 100 °C for 4 h. The activated zeolite was then magnetized with magnetite materials using the co-precipitation method described as follows. About 3 g of activated zeolite was suspended in 50 mL of 5 M NH_3 solution while stirring it with a magnetic stirrer and

heated it up to the temperature of 65 °C (solution 1). Separately, 1.4 g of $FeSO_4 \cdot 7H_2O$ and 2.7 g of $FeCl_3 \cdot 6H_2O$ (mol ratio 1:2) was dissolved in 40 mL of distilled water and stirred it for 10 min (solution 2). After the temperature of solution 1 reached 65 °C, solution 2 was added dropwise into solution 1 until a black suspension was formed. The material formed was then washed with distilled water until the solution pH was neutral. The synthesized magnetic zeolite (ZTM) was dried in an oven at 80 °C for 3 h and subjected to characterization and dithizone immobilization.

Synthesis of dithizone-immobilized magnetic zeolite

About 2 g of ZTM, 0.5 g of dithizone, and 40 mL of 1.5 M NaOH solution were mixed and stirred using a magnetic stirrer for 8 h at a temperature of 50 °C. The mixture obtained was centrifuged and washed with 0.75 M NaOH and double-distilled water until the pH of the filtrate was neutral. The solid obtained, dithizone-immobilized ZTM (ZTM-Dtz) was stored in a desiccator for 24 h and subjected to characterization and Pb(II) adsorption study.

Adsorption study

The adsorption study in this research was conducted using a batch system. Adsorption parameters, including the effect of pH, adsorbent mass, contact time, and initial concentration of Pb(II) solution were investigated. The effect of pH was carried out by interacting 20 mg ZTM or ZTM-Dtz with 25 mL of 20 mg L^{-1} Pb(II) solution and optimizing the solution pH in the range of 3 to 8. The effect of adsorbent mass was studied using a similar procedure but with adsorbent mass variation of 5, 10, 15, 20, 25, 30, and 50 mg. The adsorption kinetics model was determined from experimental data of various contact times, e.g., 5, 15, 30, 60, 90, 120, and 180 min and evaluated by pseudo-first-order in Eq. (1) and pseudo-second-order in Eq. (2).

$$\ln(q_e - q_t) = \ln q_e - k_1 t \quad (1)$$

$$\frac{t}{q_t} = \frac{1}{k_2 q_e^2} + \frac{1}{q_e} t \quad (2)$$

Plotting the value of t/q_t against t gave a slope value of $1/q_e$ and an intercept of $1/k_2 q_e^2$ at equilibrium. The k_2 value was obtained from 1/slope.

Adsorption isotherms were studied using the Langmuir in Eq. (3) and Freundlich isotherm in Eq. (4) models by analyzing the adsorption data of Pb(II) ions carried out at various concentrations of 10, 20, 40, 60, 80, and 100 ppm.

$$\frac{C_e}{q_e} = \frac{C_e}{q_{max}} + \frac{1}{q_{max} K_L} \quad (3)$$

The q_{max} and K_L values were obtained from the slope and intercept on the linear plot between C_e/q_e against C_e.

$$\log q_e = \log K_F + \frac{1}{n} \log C_e \quad (4)$$

The K_F and n values were calculated from the intercept and slope of the log q_e *versus* log C_e.

Desorption study

The Pb(II) ion that has been adsorbed on the adsorbents was then sequentially desorbed from the adsorbents using eluents with different desorption strengths, including double-distilled water, KNO_3, $HONH_2HCl$, and Na_2EDTA. The Pb(II) desorption was carried out by interacting the ZTM-Pb(II) and ZTM-Dtz-Pb(II) adsorbents successively into 20 mL of desorption eluents while shaking for 60 min. Then, the mixture was filtered and after drying in a desiccator for 2 h, the adsorbents were subjected to further desorption of Pb(II) ion using different eluents, while the filtrate obtained from each desorption agent was analyzed for metal ion content using AAS. The procedure was repeated until all desorption eluents had been used in the desorption experiments.

■ RESULTS AND DISCUSSION

FTIR Analysis

Fig. 1 shows the FTIR spectra of natural zeolite, activated natural zeolite, Fe_3O_4, ZTM, and ZTM-Dtz. The shift in the absorption band from 1049 to 1088 cm^{-1} in Fig. 1(a, b) is due to the loss of some of the Al atoms from the zeolite framework due to the dealumination process. The FTIR spectra also show that the amount of impurities is reduced. The specific absorption peak at wavenumber 586 cm^{-1} for Fe_3O_4 (Fig. 1(c)) is characteristic of the Fe–O stretching vibration, which is also seen in magnetic zeolite (Fig. 1(d)). Research by Gaffer et al. [10] has shown that the strong absorption

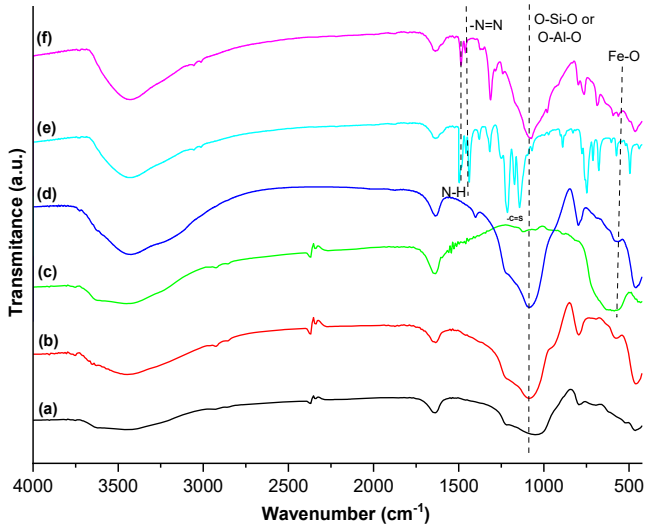

Fig 1. FTIR spectra of (a) natural zeolite, (b) activation natural zeolite, (c) Fe_3O_4, (d) ZTM, (e) dithizone, and (f) ZTM-Dtz

peak at around ~583 cm^{-1} corresponds to a typical band of nanometer-sized Fe–O covalent bond vibrations, while the position of the Fe–O vibration peak found at around ~470 cm^{-1} suggests the bulk size of Fe_3O_4. The shift in wavenumber absorption from 1088 to 1081 cm^{-1} for asymmetric stretching vibrations of O–Si–O or O–Al–O in ZTM indicates the existence of attraction or competition between Si–O groups and Fe^{2+} or Fe^{3+} in the interlayer space of zeolite [16].

The FTIR spectrum of dithizone shows absorption at 3426, 2924, 1497, 1319, 1219–1142, and 748–679 cm^{-1}, which correspond to the N–H groups, S–H groups, aromatic C=C vibrations, C=S stretching, and aromatic C–H bending vibrations, respectively. Based on the FTIR spectra in Fig. 1(e) and (f), it is observed that the FTIR spectrum of ZTM-Dtz have characteristic vibration of pure dithizone, indicating that dithizone is attached to ZTM. The new absorption bands that appear at wavenumbers 1486 and 1460 cm^{-1} are respectively, the N–H bending vibration and N=N stretching vibration of dithizone. The sharp absorption at a wavenumber of 1312 cm^{-1} indicates the stretching vibration of the C–N bond of dithizone. The C=S stretching absorption bands of dithizone at wavenumbers 1219 and 1142 cm^{-1} are not observed in ZTM-Dtz because the relatively small content of dithizone and their spectra overlap with the sharp asymmetric stretching vibrations of Si–O and Al–O at 1073 cm^{-1}. The spectrum profile in ZTM-Dtz (Fig. 1(f)) generally shows that the characteristics of zeolite and magnetite (Fig. 1(a-c) are still maintained in the zeolite framework. In addition, the characteristics of Fe_3O_4 are still visible in the spectrum, but the wavenumber has shifted from 586 to 562 cm^{-1} due to splitting stretching vibrations of the Fe–O bond [12].

XRD Analysis

The diffractogram of natural zeolite, activated natural zeolite, Fe_3O_4, ZTM, dithizone, and ZTM-Dtz are presented in Fig. 2. In general, the diffractograms of natural zeolite and activated natural zeolite as can be seen in Fig. 2(a) and (b) do not show any significant peak changes, especially at the three highest peaks at 2θ = 23, 24, and 27° which correspond to *d*-spacing 3.84, 3.57, 3.28 Å for natural zeolite and *d*-spacing 3.76, 3.57, and 3.27 Å for activated natural zeolite. By comparing the 2θ and *d*-spacing of natural zeolite and activated natural zeolite with those stored on the Crystallography Open Database (COD), it can be concluded that the mineral content in the two samples is dominated by mordenite (COD 00-230-0645). The XRD profile of activated zeolite in Fig. 2(b) shows the formation of a single sharp peak even though some of the intensities experience increases and decreases. This indicates that activation

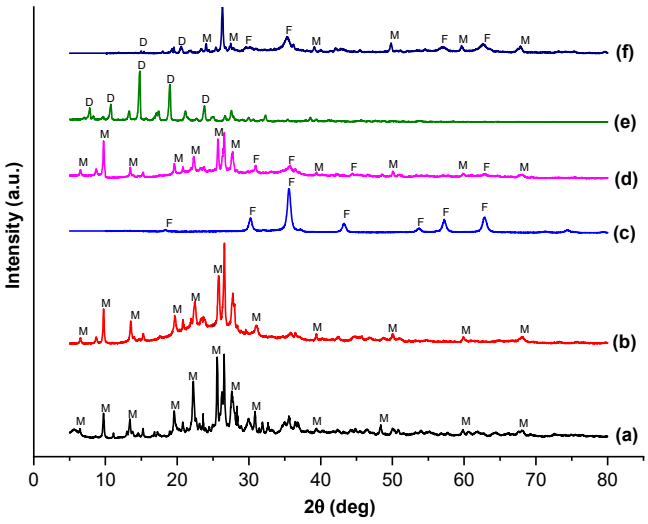

Fig 2. Diffractogram of (a) natural zeolite, (b) activation natural zeolite, (c) Fe_3O_4, (d) ZTM, (e) dithizone, and (f) ZTM-Dtz

with acid does not damage the crystal structure, instead, it removes the impurities and purifies the zeolite material [14].

The characteristic diffraction pattern for Fe_3O_4 (Fig. 2(c)) appears at 2θ of 18.37°; 30.22°; 35.60°; 43.27°; 53.68°; 57.22°; 62.84° with Miller indices of (111), (220), (311), (400), (422), (511), and (440). These peaks correspond to the magnetite phase of the inverse cubic crystal structure of spinel (COD number 00-900-5813). The ZTM (Fig. 2(d)) shows a diffraction pattern similar to the characteristics of Fe_3O_4, namely at 2θ = 30.21; 35.59°; 43.25°; 62.83°, the other peaks experienced a decrease in intensity relative to the activated zeolite. This is possible due to the large number of magnetite particles completely covering the zeolite surface, resulting in the reduced scattering intensity in Bragg reflections [15]. The decrease in intensity and the presence of a broadened peak in magnetic zeolite when compared to pure Fe_3O_4 also indicates the presence of Fe–O–Si interactions [21].

XRD analysis in ZTM-Dtz displays the existence of new 2θ peaks, namely 15.03° and 19.23°, which correspond to 2θ characteristic of dithizone (Fig. 2(e)). Fig. 2(f) shows that the mordenite peaks at 2θ, namely 13.44° and 19.59°, overlap with those of dithizone. Comparison of ZTM and ZTM-Dtz samples (Fig. 2(d) and (f)), it can be observed that the XRD intensity of the Fe peak in ZTM-Dtz is higher than that in ZTM, indicating that ZTM-Dtz has a higher degree of sample crystallinity. The high degree of crystallinity of ZTM-Dtz is influenced by the rapid nucleation or crystal growth process as a result of reaching the supersaturation point of the solution when the temperature is increased during the synthesis process [17]. Quantitative XRD analysis can be used to determine the sample size distribution using the Scherrer equation (Eq. (5));

$$D = \frac{k.\lambda}{\beta \cos\theta} \quad (5)$$

where D is the crystal grain size (nm), k is Scherrer's constant (0.89), λ is the X-ray wavelength (Kα = 1.54056 Å), β is the width at half peak (full width at half maximum = FWHM) from the main peak (radians), and θ is the peak (radians). Based on the calculation results, the crystal grain sizes of pure Fe_3O_4, ZTM, and ZTM-Dtz samples are 12.54, 17.85, and 15.65 nm, respectively. This result is lower compared to the size of Fe_3O_4 nanoparticles which ranges from ~20 to 40 nm [18] because nanoparticle size may contain more than one crystalline. Nevertheless, these observations are in agreement with the FTIR analysis data, showing the presence of nanometer-sized Fe_3O_4 particles as shown by the exhibition of Fe–O vibration peak at around ~583 nm. The data on crystal grain size can be further used to explain the magnetic properties of the two materials which are measured by VSM analysis in this study.

VSM Analysis

Based on the M-H hysteresis curve shown in Fig. 3, the three samples experience saturation when the external magnetic field H is 2T. ZTM and ZTM-Dtz samples are classified as soft magnetic materials because they provide almost symmetrical loops when subjected to a magnetic field and when the magnetic field is removed [12]. From Fig. 3, It can be observed that the saturation magnetization (M_s) values when a maximum magnetic field is applied are 60.55 emu g^{-1} for the Fe_3O_4 and 7.35 emu g^{-1} for the ZTM sample. The decrease in Ms value in ZTM relative to pure Fe_3O_4 is influenced by the presence of the Si–O layer in the ZTM composite which causes the attraction of Fe_3O_4 to the external magnet to weaken [19-20].

Meanwhile, based on Table 1 the remanent magnetization (M_r) when an external magnetic field H is

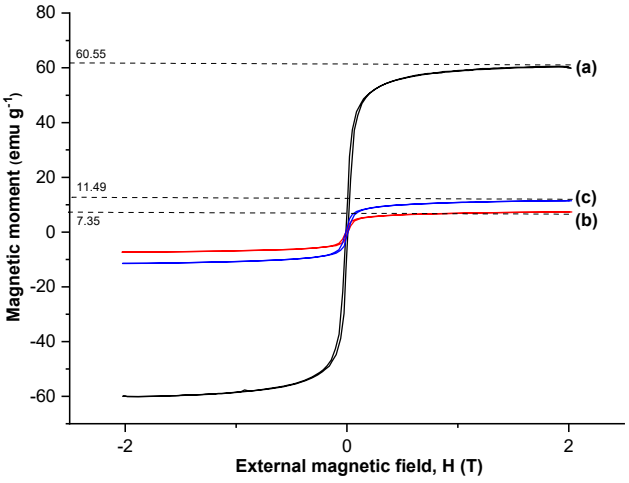

Fig 3. Magnetization curve of (a) Fe_3O_4, (b) ZTM, and (c) ZTM-Dtz

Table 1. Comparison of magnetic properties of Fe_3O_4, ZTM, and ZTM-Dtz

Sample	M_s (emu g^{-1})	M_r (emu g^{-1})	H_c (Tesla × 10^{-3})	Grain size (nm)
Fe_3O_4	60.55	6.46	8.40	12.54
ZTM	7.35	0.84	9.30	17.85
ZTM-Dtz	11.49	1.29	9.20	15.65

applied with a value of 0 for sample (a) is 6.46 emu g^{-1} and sample (b) is 0.84 emu g^{-1} and the value of coercivity field (H_c) in the sample (a) is 0.0084 T and sample (b) 0.0093 T. The analysis results show that the reduction in the coercivity field is proportional to the decrease in nanoparticle grain size. Referring to Table 1, the M_s value for the ZTM is 7.35 emu g^{-1} and for ZTM-Dtz is 11.49 emu g^{-1}. The M_r value for ZTM is 0.84 emu g^{-1} and ZTM-Dtz is 1.29 emu g^{-1}. The coercivity field values (H_c) in the ZTM and ZTM-Dtz are 0.0093 and 0.0092 T, respectively. The increase in the value of M_s to a larger value after the composite was modified with dithizone can be attributed to the presence of dithizone functional groups which play a role in limiting the growth rate of Fe_3O_4 and preventing agglomeration due to its strong chelation of Fe^{3+} and Fe^{2+}. Consequently, the crystal size of the composite will be smaller and its degree of crystallinity increases as can be seen from the XRD diffractogram given in Fig. 2 [19]. Based on Rampengan and Tengker [22] and Prasetyowati et al. [23], ZTM and ZTM-Dtz materials are classified as soft magnetic materials because they have relatively low M_r value and H_c.

Adsorption Study

Effect of solution pH on Pb(II) adsorption

The solution pH affects the charge of the adsorbent active site as well as the speciation of adsorbate in the solution. Based on Fig. 4, the amount of Pb(II) ions adsorbed by the adsorbents increases with the increase of the solution pH. After reaching the optimum pH, the adsorption tends to be constant or a little bit decreases. As can be seen in general adsorption of Pb(II) with either ZTM or ZTM-Dtz reaches their optimal condition at pH 5–7.

Under acidic conditions (pH < 4), the proton (H^+) content increases so that protonation occurs on the surface of the adsorbent to form positively charged active sites which induces repulsion with positively charged Pb(II) ions. Moreover, a Pb(II) solution with a concentration of 20 mg L^{-1} (9.66×10^{-5} M) will theoretically form a $Pb(OH)_2$ precipitate at a pH of around 8.54 ($K_{sp} = 1.2 \times 10^{-15}$). As the pH increases (pH > 7), Pb^{2+} and $Pb(OH)^+$ species in the solution decrease. On the other hand, the adsorbent surface will experience deprotonation to give a partially negative charge of the active sites. However, increasing the concentration of OH^- ions causes the formation of $Pb(OH)_2$ hydroxide precipitates, or negatively charged Pb species $Pb(OH)_3^-$ and $Pb_3(OH)_4^{2-}$, therefore the interaction of the adsorbent with Pb(II) decreases due to electrostatic repulsion and the formation of precipitates [24-25].

From the results of this research, it is obtained that the optimum pH for adsorption of Pb(II) ions on ZTM and ZTM-Dtz adsorbents is at pH 6 and 5 respectively and these pH has been used for further adsorption studies of Pb(II). This optimum pH may be explained by considering the point zero charge (pzc) value of magnetic zeolite. It has been reported that magnetic zeolite with

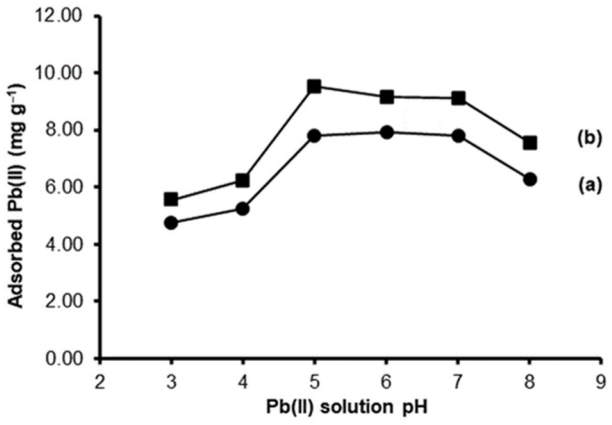

Fig 4. Effect of solution pH on the adsorption of Pb(II) ions by (a) ZTM and (b) ZTM-Dtz

a Fe_3O_4 fraction of 33.3% w/w has a pH_{pzc} value of 3.5 [26]. If the solution is at a pH higher than pH_{pzc}, the ZTM active site will be negatively charged and its interaction with the positive metal ion Pb^{2+} through ion exchange or electrostatic interaction will be favorable. Pambudi et al. [8] explained that at a medium pH of around pH 6, the main species of Pb(II) is Pb^{2+} with the $Pb(OH)^+$ complex starting to form. Meanwhile, the adsorption of Pb(II) ions with the ZTM-Dtz adsorbent reaches a maximum point at pH 5. According to Gracias et al. [27], at pH 5, an equilibrium reaction has occurred between the metal ion (M^{2+}) and dithizone (H_2Dz) which leads to the formation of a metal-dithizonate complex. The reaction equation for the formation of the dithizonate complex is given in Eq. (6).

$$M^{n+} + H_2O + nH_2Dz \rightleftharpoons M(HDz) + nH_3O^+ \quad (6)$$

Apart from that, it can also be explained that the dissociation constant (pKa_1) value of dithizone is in the range of 4.0–4.5, which means that at pH > 4.5 dithizone has been ionized to become HDz^- making it easier to form chelate complexes with metal ions. The higher ability of ZTM-Dtz in adsorbing Pb(II) ions compared to ZTM can also be explained by the hard soft acid base (HSAB) principle. ZTM-Dtz has active groups of –NH and –SH which are classified as medium and soft bases so their interaction with the medium acid of Pb(II) ions is stronger involving covalent bond formation hence, it is not surprising that Pb(II) is much more adsorbed by ZTM-Dtz rather than by ZTM.

Effect of adsorbent mass

The mass of the adsorbent is directly related to the number of adsorbent active sites in the solution. The effect of adsorbent mass on the adsorption of Pb(II) ions for ZTM and ZTM-Dtz adsorbents is presented in Fig. 5. It can be seen from Fig. 5 that the amount of Pb(II) ions absorbed increases with increasing adsorbent mass in the range of 10–20 mg either for ZTM or ZTM-Dtz until it reaches the optimum point at a mass of 20 mg. The increase in adsorption of Pb(II) is due to the increase in the number of adsorbent active sites that can interact with Pb(II) ions in the solution. However, further increasing of adsorbent mass, e.g. > 20 mg has no significant changes in the amount of adsorbed Pb(II) because the adsorbent-adsorbate equilibrium had been reached. In fact, the adsorption of Pb(II) tends to experience a slight decrease because the excessive amount of adsorbent mass may induce the formation of aggregates that can cover the active site of the adsorbent [28].

Kinetic study of Pb(II) adsorption

Fig. 6 gives the experimental results about the effect of contact time on the adsorption of Pb(II). It can be observed from this figure that the increasing contact time results in the higher the adsorption capacity. This is because the interaction probability between the active groups of the adsorbent and the Pb(II) metal ion becomes larger as the contact time increases, giving rise to the higher amount of Pb(II) ions that can be adsorbed. In the beginning, the adsorption of Pb(II) ions on ZTM and ZTM-DTz adsorbents increased rapidly up to 30 min of contact time, afterwards the adsorption rate

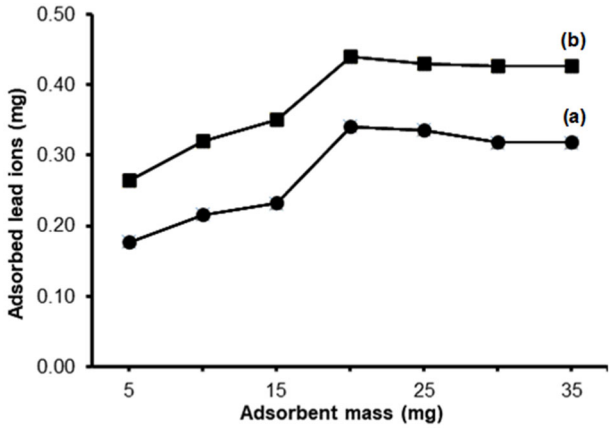

Fig 5. Effect of adsorbent mass on the adsorption ability of Pb(II) ions on (a) ZTM and (b) ZTM-Dtz

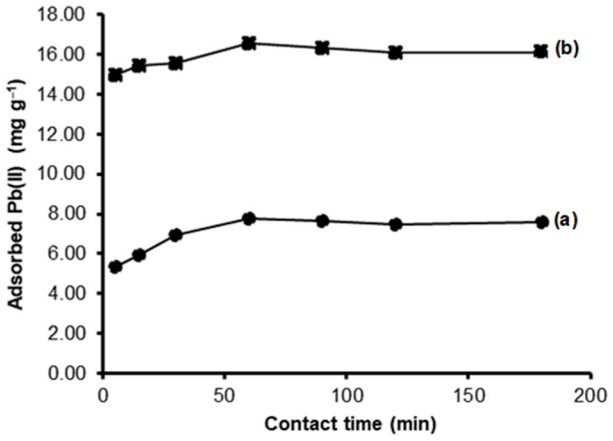

Fig 6. Effect of contact time on the adsorption of Pb(II) metal ions by (a) ZTM and (b) ZTM-Dtz

increased more slowly until the equilibrium point was reached at a contact time of 60 min. After reaching the optimum point, the adsorption capacity tends to be constant or even decreases slightly. This is probably due to the saturation of the adsorbent surface with ion Pb(II) or the solution mixture has reached the equilibrium between the active site and the Pb(II) ion. In addition, long interaction times accompanied by continuous stirring after the optimum time has been reached may cause some of the metal ions that have been adsorbed to be re-released to yield a slight decrease in the Pb(II) adsorption [28]. The adsorption kinetic parameters of Pb(II) on ZTM and ZTM-Dtz are then evaluated using a pseudo-first-order kinetic model approach according to Lagergren or Ho & McKay and the results are presented in Table 2.

Experimental results show that the pseudo-second-order kinetic model is more suitable for both adsorbents because it provides an adsorption capacity (q_e) that is more in line with experimental data and from the correlation coefficient it has a value of R^2 closer to unity ($R^2 > 0.99$). The pseudo-second-order kinetic model implies that the adsorption rate is proportional to the squared number of adsorption active sites [29]. The adsorption process occurs at certain active sites or is localized on the surface of the adsorbent, meaning that the adsorption rate involves chemical mechanisms (chemisorption) by forming covalent interactions or ion exchange [26]. Based on Table 2, the adsorption rate constant (k_2) and the amount of Pb(II) ions adsorbed at equilibrium (q_e) obtained from the ZTM-Dtz adsorbent have values higher than those of ZTM. These results are in line with the research results that have been previously reported [9,27-28]. It is clearly seen from these results that the immobilization of dithizone provides additional active groups –NH and –SH on the surface of the adsorbent.

Isotherm study of Pb(II) adsorption

The adsorption isotherm describes the relationship between the concentration of adsorbate remaining in the solution phase and that adsorbed on the surface of the solid at a given temperature after equilibrium has been reached [30]. In this study, the adsorption isotherm has been evaluated using the Langmuir and Freundlich isotherm models by analyzing Pb(II) adsorption data carried out at various concentrations, namely 10, 20, 40, 60, 80, and 100 ppm. The adsorption conditions were set in accordance with the optimum conditions obtained from previous experiments, i.e. pH 6 for ZTM, pH 5 for ZTM-Dtz, 20 mg of the adsorbent mass, and contact time of 60 min. Based on Fig. 7, the amount of Pb(II) metal ions adsorbed increases along with the increase in the initial adsorbate concentration until it reaches the optimum condition of 80 ppm.

At low concentrations, almost all Pb(II) metal ions are adsorbed on the surface of the adsorbent because the active sites are still abundant compared to the amount of Pb(II) ion and it continues to increase until it reaches the

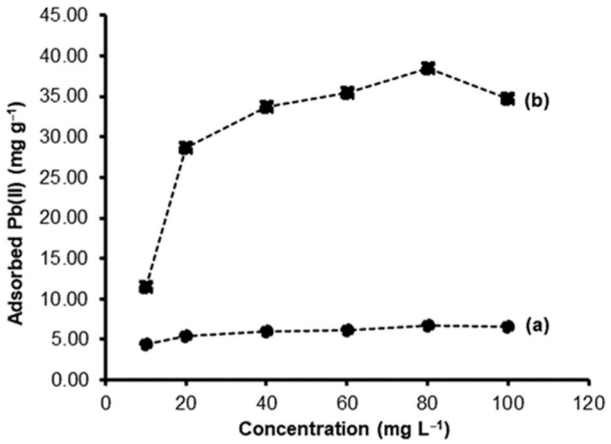

Fig 7. Effect of initial concentration on the adsorption capacity of Pb(II) ions adsorbed by (a) ZTM and (b) ZTM-Dtz

Table 2. Kinetic parameters of Pb(II) adsorption on ZTM and ZTM-Dtz

Adsorbent	Pseudo-first-order			Pseudo-second-order		
	q_e (mg g^{-1})	k_1 (min^{-1})	R^2	q_e (mg g^{-1})	k_2 (g mg^{-1} min^{-1})	R^2
ZTM	1.746	0.015	0.707	7.680	0.055	0.999
ZTM-Dtz	1.218	0.008	0.537	16.207	0.276	0.999

equilibrium point. After the optimum concentration, the adsorption capacity is almost constant because the active sites on the adsorbent surface have been saturated, so further increasing the adsorbate concentration does not affect the amount of adsorbed Pb(II) ions. The Langmuir and Freundlich isotherm parameters obtained from this study are presented in Table 3. Based on these results, Langmuir isotherm model is more appropriate to describe the adsorption process of Pb(II) ions either by ZTM or ZTM-Dtz.

The Langmuir isotherm model assumes that the active sites on the surface of the adsorbent are homogeneous so that forming a single layer (monolayer) or in other words the adsorption process occurs through a chemical mechanism between one active site on the adsorbent surface and one adsorbate molecule. The Langmuir constant (K_L) values can be further used to determine the adsorption energy (E_{ads}). The value of adsorption energy is then used to predict the mechanism of interactions, e.g. physical interactions (physisorption), chemical interactions (chemisorption), or a mixture of both. According to Adamson [31], the adsorption energy value of physisorption is less than 20.92 kJ mol^{-1}, while the adsorption energy of chemical interaction is more than 20.92 kJ mol^{-1}. The adsorption energy value is equivalent to the negative value of the change in Gibbs free energy which is written according to Eq. (7).

$$E_{ads} = -\Delta G^\circ = RT\ln K \quad (7)$$

Results of the calculation suggest that the adsorption energy of Pb(II) ions either by ZTM or ZTM-Dtz is more than 20.92 kJ mol^{-1}, indicating that the adsorption can be categorized as chemical interaction (chemisorption). The adsorption process most likely involves electrostatic interactions, hydrogen bonds, and coordinating covalent bonds [28]. The isotherm parameter of Pb(II) was comparable with the different adsorbents reported in previous papers in Table 4.

According to Langmuir model, the maximum adsorption capacity (q_{max}) of Pb(II) for ZTM and ZTM-Dtz are 6.94 and 38.46 mg g^{-1}, respectively, indicating that q_{max} has increased about 5 times due to the immobilization of dithizone. The presence of additional functional groups of –NH and –SH from dithizone increases significantly the adsorption ability of the adsorbent towards Pb(II) ions. In addition to giving an increasing effect in q_{max}, the immobilization of dithizone also provides more stable complex formation of adsorbent-adsorbate. From Table 4, it can be observed that the E_{ads} value obtained is higher [33-34,36] or comparable [29,35] to the previously reported results.

Table 3. Parameters of Langmuir and Freundlich adsorption isotherms on the adsorption of Pb(II) ions by ZTM and ZTM-Dtz

Adsorbent	Isoterm Langmuir			Isoterm Freundlich			
	q_m (mg g^{-1})	K_L (L mg^{-1})	R^2	K_F (mg g^{-1})	N	R^2	E_{ads} (kJ mol^{-1})
ZTM	6.944	0.183	0.997	3.267	6.305	0.961	26.560
ZTM-Dtz	38.462	0.535	0.993	15.985	4.771	0.579	29.260

Table 4. Comparison of isotherm parameters with various types of adsorbents on the adsorption of Pb(II) ions reported in the literature

Adsorbents	q_m (mg g^{-1})	E_{ads} (kJ mol^{-1})	Ref
Nanoadsorbent of Oryza sativa husk	6.10	13.06	[32]
Oil Palm Bio-Waste/MWCNTs/PVA hydrogel	30.03	17.56	[33]
Dtz-Coal bottom ash	31.25	36.25	[29]
Coal fly ash-dithizone	31.61	31.74	[34]
HCO-$(Fe_3O_4)_x$ composite	28.27	26.15	[35]
ZTM	6.94	26.56	This study
ZTM-Dtz	38.46	29.26	This study

Detailed examination of Table 4, it is revealed that the E_{ads} value of ZTM-Dtz is slightly higher than that of ZTM as the effect of Dtz immobilization, but both of them are classified as chemical interactions. The different values of E_{ads} for several types of adsorbents that used dithizone as a ligand suggest that interaction between the active sites of adsorbent and Pb(II) ion is also dependent on the type of supporting material used as a host.

Identification of the Type of Pb(II) Interaction by Sequential Desorption

The results of the sequential desorption experiment of Pb(II) metal ions from ZTM and ZTM-Dtz adsorbents are presented in Fig. 8. Based on the experimental results, it can be observed that the contribution of the physical interaction (desorption using H_2O) between Pb(II) metal ion and the two adsorbents is relatively low. This is due to the presence of stronger active groups either on ZTM or ZTM-Dtz such as Si–OH, Al–OH, Si–O–Si, Fe–OH, –NH and –SH which can interact more dominantly with Pb(II) metal ions through chemical interactions than physical interaction.

The interaction between Pb(II) ions and the ZTM adsorbent is dominated by ion exchange or electrostatics (desorption by KNO_3) with relative desorption reaching 78.47%. Electrostatic interactions can be driven by cation exchange where metal ions replace protons (H^+) from the adsorption site. This result can also be explained with respect to the optimum pH of the adsorption (pH 6). This pH is higher than the pH_{PZC} of the ZTM material, meaning that the surface of the adsorbent has a negative charge that allows electrostatic attraction to occur with the positively charged Pb(II) species [27].

The results of Pb(II) sequential desorption from the ZTM-Dtz indicate a decrease in the contribution of electrostatic interactions to 24.30% from the original of 78.47%. Instead, the interaction of Pb(II) with ZTM-Dtz is dominated by hydrogen bonds (40.10%) and the formation of dithizonate complex compounds (34.87%). The change in the interaction mechanism of the Pb(II) metal ion from ion exchange to hydrogen bonding is not surprising as the Pb(II) species in water does not stand alone but it is in the form of a hydrated complex. The presence of the H_2O ligand around the Pb(II) metal ion can be a link for the formation of hydrogen bonds between the active site of the adsorbent and the Pb(II) ion.

The use of Na_2EDTA to desorb metal ions bound to the adsorbent through the formation of complex compounds is based on the strong properties of EDTA as a ligand. Hence, it can release Pb(II) ion that bound to adsorbent active groups [27]. Covalent bonds are predicted to occur between the dithizone active groups of –NH and –SH, which are categorized as medium and soft bases, and the Pb(II) ion which is a medium acid according to the HSAB classification to form a stable dithizonate complex [28].

Based on the results of sequential desorption studies, most of the interactions involved in the adsorption of Pb(II) ions by the two adsorbents are chemical interactions (chemisorption). The interactions in ZTM are dominated by electrostatic interactions or ion exchange while in ZTM-Dtz it involves hydrogen bonds and the formation of metal complex by sharing of electron pairs. These results agree very well with the Langmuir isotherm model suggesting that the adsorption process occurs through a chemical mechanism (chemisorption). Hypothetical interactions that may occur between Pb(II) ions and ZTM and ZTM-Dtz adsorbents are presented in Fig. 9 and 10 [9,36].

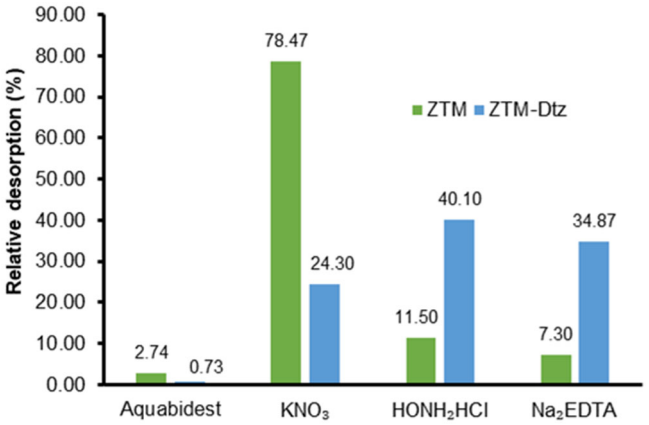

Fig 8. Sequential desorption of Pb(II) metal ions from ZTM and ZTM-Dtz using various desorption solutions

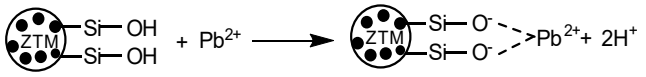

Fig 9. Prediction of ion exchange interaction between Pb(II) metal ion and ZTM

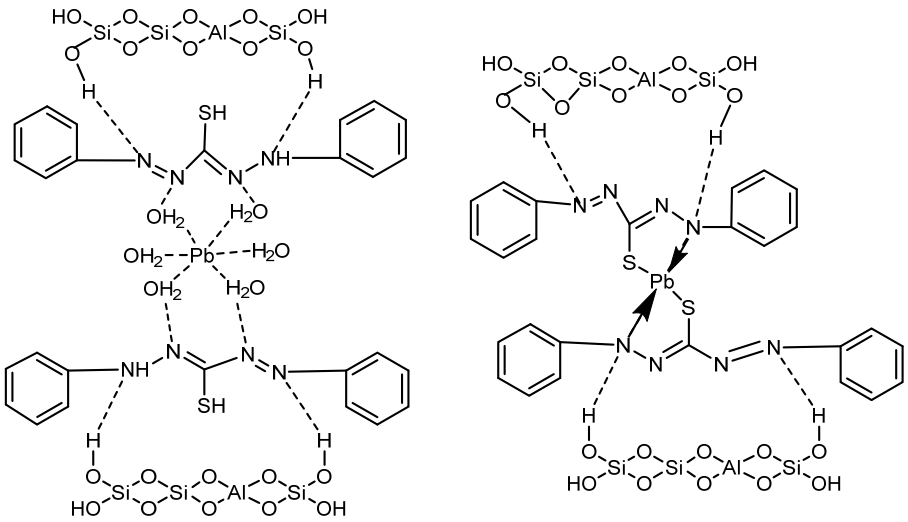

Fig 10. Prediction of the interaction of Pb(II) metal ion with ZTM-Dtz (a) hydrogen bond and (b) complexation

■ CONCLUSION

Based on the FTIR and XRD characterization results, it has been shown that dithizone is successfully immobilized on magnetized zeolite possibly through the hydrogen bonds interaction between the –OH active group of silanol and the –NH active group of dithizone to give ZTM-Dtz. Both ZTM and ZTM-Dtz adsorbents showed superparamagnetic properties with M_s values of 7.35 and 11.49 emu g^{-1} respectively. The adsorption kinetics of Pb(II) ions on ZTM and ZTM-Dtz adsorbents follow a pseudo-second-order kinetic model with the adsorption rate constant (k_2) on ZTM-Dtz being higher than ZTM. Adsorption of Pb(II) metal ions on both adsorbents follows the Langmuir isotherm model with the adsorption capacity and Langmuir constant (K_L) values for ZTM-Dtz extremely higher than that of ZTM. As expected, the type of interactions involved in the adsorption process of Pb(II) ions by ZTM is dominated by electrostatic interactions while that in ZTM-Dtz are dominated by hydrogen bonds and complexation due to the presence of dithizone. The developed adsorbent is prospective to be used in the removal of Pb(II) from waters as its capacity and selectivity are enhanced and can be easily separated from the mixture solution using an external magnet. This adsorbent may also be promising to be applied to other heavy metal ions such as Cd(II), Hg(II), and Cu(II) because the immobilized dithizone can selectively form a metal chelate with those metal ions.

■ ACKNOWLEDGMENTS

The first author (CAS) would like to acknowledge the Ministry of Education, Culture, Research and Technology of the Republic of Indonesia for the financial support through "*Beasiswa Unggulan*" for M.Sc. program in Chemistry at Universitas Gadjah Mada under contract number No. 0348/J5.2.2/BP/PKS/2022 dated 22 November 2022.

■ CONFLICT OF INTEREST

The authors declare that they have no conflict of interest.

■ AUTHOR CONTRIBUTIONS

Carissa Ayu Susiana and Mudasir were involved in conceptualization, funding acquisition, resources, formal analysis, investigation, and writing-original draft. Mudasir and Bambang Rusdiarso conducted supervision, methodology, validation, writing-review, and editing. All authors agreed to the final version of this manuscript.

■ REFERENCES

[1] Kumar, A., Kumar, A., Cabral-Pinto, M., Chaturvedi, A.K., Shabnam, A.A., Subrahmanyam, G., Mondal, R., Gupta, D.K., Malyan, S.K., Kumar, S.S., Khan, S.A., and Yadav, K.K., 2020, Lead toxicity: Health hazards, influence on food chain,

and sustainable remediation approaches, *Int. J. Environ. Res. Public Health*, 17 (7), 2179.

[2] Balali-Mood, M., Naseri, K., Tahergorabi, Z., Khazdair, M.R., and Sadeghi, M., 2021, Toxic mechanisms of five heavy metals: Mercury, lead, chromium, cadmium, and arsenic, *Front. Pharmacol.*, 12, 643972.

[3] Gazwi, H.S.S., Yassien, E.E., and Hassan, H.M., 2020, Mitigation of lead neurotoxicity by the ethanolic extract of Laurus leaf in rats, *Ecotoxicol. Environ. Saf.*, 192, 110297.

[4] Renu, R., Agarwal, M., and Singh, K., 2017, Methodologies for removal of heavy metal ions from wastewater: An overview, *Interdiscip. Environ. Rev.*, 18 (2), 124–142.

[5] Türkmen, D., Bakhshpour, M., Akgönüllü, S., Aşır, S., and Denizli, A., 2022, Heavy metal ions removal from wastewater using cryogels: A review, *Front. Sustainability*, 3, 765592.

[6] Kozlenko, D.P., Dubrovinsky, L.S., Kichanov, S.E., Lukin, E.V., Cerantola, V., Chumakov, A.I., and Savenko, B.N., 2019, Magnetic and electronic properties of magnetite across the high pressure anomaly, *Sci. Rep.*, 9 (1), 4464.

[7] Wang, C., Leng, S., Guo, H., Cao, L., and Huang, J., 2019, Acid and alkali treatments for regulation of hydrophilicity/hydrophobicity of natural zeolite, *Appl. Surf. Sci.*, 478, 319–326.

[8] Pambudi, T., Wahyuni, E.T., and Mudasir, M., 2020, Recoverable adsorbent of natural zeolite/Fe_3O_4 for removal of Pb(II) in water, *J. Mater. Environ. Sci.*, 11 (1), 69–78.

[9] Huda, B.N., Wahyuni, E.T., and Mudasir, M., 2023, Simultaneous adsorption of Pb(II) and Cd(II) in the presence of Mg(II) ion using eco-friendly immobilized dithizone on coal bottom ash, *S. Afr. J. Chem. Eng.*, 45, 315–327.

[10] Gaffer, A., Al Kahlawy, A.A., and Aman, D., 2017, Magnetic zeolite-natural polymer composite for adsorption of chromium(VI), *Egypt. J. Pet.*, 26 (4), 995–999.

[11] Ntoi, L.L.A., Buitendach, B.E., and von Eschwege, K.G., 2017, Seven chromisms associated with dithizone, *J. Phys. Chem. A*, 121 (48), 9243–9251.

[12] Gogoi, A., Navgire, M., Sarma, K.C., and Gogoi, P., 2017, Novel highly stable β-cyclodextrin fullerene mixed valent Fe-metal framework for quick Fenton degradation of alizarin, *RSC Adv.*, 7 (64), 40371–40382.

[13] Ivanković, A., Dronjić, A., Bevanda, A.M., and Talić, S., 2017, Review of 12 principles of green chemistry in practice, *Int. J. Sustainable Green Energy*, 6 (3), 39–48.

[14] Triyono, T., Trisunaryanti, W., Putri, Y.W., Fatmawati, D.A., and Chasanah, U., 2021, Modification of mordenite characters by $H_2C_2O_4$ and/or NaOH treatments and its catalytic activity test in hydrotreating of pyrolyzed α-cellulose, *Bull. Chem. React. Eng. Catal.*, 16 (1), 9–21.

[15] Rendo, D., 2021, Adsorption of methylene blue dye using Fe_3O_4 magnetized natural zeolite adsorbent, *J. Kim. Sains Apl.*, 24 (2), 51–57.

[16] Buzukashvili, S., Hu, W., Sommerville, R., Brooks, O., Kökkılıç, O., Rowson, N.A., Ouzilleau, P., and Waters, K.E., 2023, Magnetic zeolite: Synthesis and copper adsorption followed by magnetic separation from treated water, *Crystals*, 13 (9), 1369.

[17] Cashmore, A., Miller, R., Jolliffe, H., Brown, C.J., Lee, M., Haw, M.D., and Sefcik, J., 2023, Rapid assessment of crystal nucleation and growth kinetics: Comparison of seeded and unseeded experiments, *Cryst. Growth Des.*, 23 (7), 4779–4790.

[18] Sun, S.N., Wei, C., Zhu, Z.Z., Hou, Y.L., Venkatraman, S.S., and Xu, Z.C., 2014, Magnetic iron oxide nanoparticles: Synthesis and surface coating techniques for biomedical applications, *Chin. Phys. B*, 23 (3), 037503.

[19] Storozhuk, L., and Iukhymenko, N., 2019, Iron oxide nanoparticles modified with silanes for hyperthermia applications, *Appl. Nanosci.*, 9 (5), 889–898.

[20] Elwakeel, K.Z., Hamza, M.F., and Guibal, E., 2021, Effect of agitation mode (mechanical, ultrasound and microwave) on uranium sorption using amine- and dithizone-functionalized magnetic chitosan hybrid materials, *Chem. Eng. J.*, 411, 128553.

[21] Dhahawi Ahmad, A.R., Imam, S.S., Oh, W.D., and Adnan, R., 2020, Fe_3O_4-zeolite hybrid material as

hetero-Fenton catalyst for enhanced degradation of aqueous ofloxacin solution, *Catalysts*, 10 (11), 1241.

[22] Rampengan, A.M., and Tengker, S.M.T., 2021, Analisa sifat kemagnetan polimer poliethylen glycol (PEG-4000)-coated nanopartikel magnetite Fe_3O_4 menggunakan vibrating sample magnetometer (VSM), *Fullerene J. Chem.*, 6 (2), 161–164.

[23] Prasetyowati, R., Widiawati, D., Swastika, E., and Ariswan, W., 2021, Sintesis dan karakterisasi nanopartikel magnetit (Fe_3O_4) berbasis pasir besi pantai Glagah Kulon Progo dengan metode kopresipitasi pada berbagai variasi konsentrasi NH_4OH, *J. Sains Dasar*, 10 (2), 57–61.

[24] Caccin, M., Giorgi, M., Giacobbo, F., Da Ros, M., Besozzi, L., and Mariani, M., 2016, Removal of lead (II) from aqueous solutions by adsorption onto activated carbons prepared from coconut shell, *Desalin. Water Treat.*, 57 (10), 4557–4575.

[25] Huang, J., Yuan, F., Zeng, G., Li, X., Gu, Y., Shi, L., Liu, W., and Shi, Y., 2017, Influence of pH on heavy metal speciation and removal from wastewater using micellar-enhanced ultrafiltration, *Chemosphere*, 173, 199–206.

[26] Asanu, M., Beyene, D., and Befekadu, A., 2022, Removal of hexavalent chromium from aqueous solutions using natural zeolite coated with magnetic nanoparticles: Optimization, kinetics, and equilibrium studies, *Adsorpt. Sci. Technol.*, 2022, 8625489.

[27] Gracias, W., Huda, B.N., Suratman, A., and Mudasir, M., 2022, Immobilization of dithizone on magnetic zeolite in less toxic medium and its application as adsorbent Cd(II) ion in water, *Mater. Sci. Forum*, 1076, 133–142.

[28] Aminy, D.E., Rusdiarso, B., and Mudasir, M., 2022, Adsorption of Cd(II) ion from the solution using selective adsorbent of dithizone-modified commercial bentonite, *Int. J. Environ. Sci. Technol.*, 19 (7), 6399–6410.

[29] Huda, B.N., Wahyuni, E.T., Kamiya, Y., and Mudasir, M., 2022, Kinetic and thermodynamic study on adsorption of lead(II) ions in water over dithizone-immobilized coal bottom ash, *Mater. Chem. Phys.*, 282, 126005.

[30] Neolaka, Y.A.B., Lawa, Y., Naat, J., Riwu, A.A.P., Mango, A.W., Darmokoesoemo, H., Widyaningrum, B.A., Iqbal, M., and Kusuma, H.S., 2022, Efficiency of activated natural zeolite-based magnetic composite (ANZ-Fe_3O_4) as a novel adsorbent for removal of Cr(VI) from wastewater, *J. Mater. Res. Technol.*, 18, 2896–2909.

[31] Adamson, A.W., 1990, *Physical Chemistry of Surfaces*, John Wiley & Sons, New York, US.

[32] Kaur, M., Kumari, S., and Sharma, P., 2020, Removal of Pb(II) from aqueous solution using nanoadsorbent of *Oryza sativa* husk: Isotherm, kinetic and thermodynamic studies, *Biotechnol. Rep.*, 25, e00410.

[33] Zulfiqar, M., Lee, S.Y., Mafize, A.A., Abdul Kahar, N.A.M., Johari, K., and Rabat, N.E., 2020, Efficient removal of Pb(II) from aqueous solutions by using oil palm bio-waste/MWCNTs reinforced PVA hydrogel composites: Kinetic, isotherm and thermodynamic modeling, *Polymers*, 12 (2), 430.

[34] Fitriana, D., Mudasir, M., and Siswanta, D., 2020, Adsorption of Pb(II) from aqueous solutions on dithizone-immobilized coal fly ash, *Key Eng. Mater.*, 840, 57–63.

[35] Li, J., Hu, Z., Chen, Y., and Deng, R., 2023, Removal of Pb(II) by adsorption of HCO–$(Fe_3O_4)_x$ composite adsorbent: Efficacy and mechanism, *Water*, 15 (10), 1857.

[36] Sočo, E., and Kalembkiewicz, J., 2013, Adsorption of nickel(II) and copper(II) ions from aqueous solution by coal fly ash, *J. Environ. Chem. Eng.*, 1 (3), 581–588.